THE JOURNAL OF BIOLOGICAL CHEMISTRY

Vol. 269, No. 18, Issue of May 6, pp. 13353-13360, 1994
Printed in U.S.A.

Analysis of Microtubule Rigidity Using Hydrodynamic Flow and Thermal Fluctuations*

(Received for publication, November 18, 1993, and in revised form, January 28, 1994)

Pascal Venier, Anthony C. Maggs‡, Marie-France Carlier, and Dominique Pantaloni

From the Laboratoire d'Enzymologie, CNRS, 91198 Gif-sur-Yvette Cedex, France and the ‡Groupe de Physico-Chimie Théorique, Ecole Supérieure de Physique et de Chimie Industrielles de la Ville de Paris, 10 rue Vanquelin, F 75231 Paris Cedex 05, France

We report the use of two independent new methods to measure the flexural rigidity of microtubules. Microtubules were grown off axonemal pieces adhering to a glass coverslip. In the first method, a hydrodynamic flow was applied to microtubules and the flexural rigidity was derived from the analysis of the bending shape of the microtubules at equilibrium in the flow. In the second method, the flexural rigidity was derived from the thermal fluctuations of the free end of axoneme-bound microtubules.

With both methods, the flexural rigidity of standard GDP microtubules was estimated to be $0.85 \pm 0.2 \times 10^{-23}$ newtons × m^2 which corresponded to a persistence length of 2 ± 0.2 mm. Binding of ligands known to affect the biochemical properties of microtubules affected their rigidity. The structural analogs of inorganic phosphate AlF_4^- and $[BeF_3^-, H_2O]$, which bind to the site of the γ-phosphate of GTP on GDP microtubule and reconstitute the GDP-P_i microtubule intermediate state of GTP hydrolysis, cause an ~3-fold increase in microtubule flexural rigidity and persistence length. Taxol and taxotere, antitumoral microtubule-stabilizing drugs, in contrast cause a decrease in flexural rigidity and appear to affect the three-dimensional superstructure of microtubules, which can no longer be considered as semi-flexible rods. The relationship between the mechanical properties of microtubules and their biological function is discussed.

Microtubules are a major component of the cytoskeleton of eukaryotic cells. These fibrous polymers form the architecture of the cell. They define the spatial distribution of most organelles (*e.g.* the Golgi, the endoplasmic reticulum), are used as tracks for dynein- and kinesin-directed vesicular transport and support the movement of chromosomes toward the poles in mitosis. Microtubule biological functions rely on two essential properties. First, they are dynamic polymers that are assembled and disassembled rapidly in a fashion concerted with motile reactions; second, they are relatively rigid structures able to resist the ~1 piconewton forces exerted by kinesin and dynein, and to maintain the stiffness of cilia and flagella. The rigidity of microtubules, apprehended from their straight shape in the electron microscope (1) and in video microscopy observations (2–4), is due to their structure of hollow cylinders made of the parallel arrangement of 13 adjacent protofilaments, forming a bidimensional lattice within which tubulin subunits interact with each other through lateral and longitudinal bonds (5–7). It is known that the stability of tubulin-tubulin interactions in the microtubule is regulated by GTP hydrolysis associated to microtubule assembly (8), and by the binding of microtubule-associated proteins (9) or of drugs such as taxol (10). On the other hand, whether the mechanical properties of microtubules are regulated *in vivo* and whether changes in flexibility affect microtubule functions is less well known. Recently, a thorough, quantitative study of microtubule flexural rigidity (11) has been carried out, using dark-field and fluorescence video-enhanced microscopy to monitor the thermal fluctuations in shape of microtubules free in solution. The results of this analysis showed that taxol-stabilized microtubules had a persistence length, L_p, of 5,200 μm and a Young's modulus, E, of 1.2 gigapascals, while preliminary data obtained in the absence of taxol led to lower values ($L_p \sim 1000$ μm) for standard microtubules. The stiffening of microtubule structure by taxol described in that study contrasts with the recent report (12) that taxol induces a higher flexibility of microtubules, as observed in a flow of buffer. Binding of microtubule-associated proteins, in the same work (12), was found to increase the rigidity of microtubules.

In the present work, we have used two novel methods to determine the physical parameters of microtubule flexibility. Dark-field video-microscopy was used to observe individual microtubules attached by one end to axonemal pieces fixed on the glass. In the first method, the bending shape of microtubules in a hydrodynamic flow was analyzed quantitatively. In the second static method, the persistence length was derived from measurements of the thermal fluctuations of the free end of microtubules attached to axonemes by the other end. Two main goals were sought. Because each physical method possesses its inherent biases and artifacts, it was useful to compare the results obtained using these new techniques with previous data. Second, microtubule ligands whose biochemical properties are known were assayed for their effect on microtubule flexibility. The structural analogs of P_i, BeF_3^-, H_2O, and AlF_4^-, which are known to stabilize microtubules in the GDP-P_i intermediate state of GTP hydrolysis (13), were found to stiffen microtubules; in contrast, taxol and its analog taxotere (14) increase microtubule flexibility and induce a large change in the three-dimensional structure of microtubules, which can no longer be considered as rods.

The results help to resolve reported discrepancies concerning the effect of taxol and provide new insight in the regulation of microtubule function by GTP hydrolysis.

MATERIALS AND METHODS

Chemicals—MES[1] and PIPES were from Calbiochem, EGTA from Sigma, beryllium sulfate tetrahydrate and aluminum nitrate (gold la-

* This work was supported in part by the Association pour la Recherche contre le Cancer (ARC), the Ligue Nationale Française contre le Cancer, and the Association Française contre les Myopathies (AFM). The costs of publication of this article were defrayed in part by the payment of page charges. This article must therefore be hereby marked "*advertisement*" in accordance with 18 U.S.C. Section 1734 solely to indicate this fact.

[1] The abbreviations used are: MES, 2-(*N*-morpholino)ethanesulfonic acid; PIPES, piperazine-*N*,*N*'-bis(2-ethanesulfonic acid); N, newton(s).

bel) from Aldrich, and GTP from Boehringer. Taxol was a gift from Dr. D. Guénard (Gif-sur-Yvette, France) and taxotere^R was obtained from Rhône-Poulenc-Rorer Company.

Tubulin—Tubulin was purified from pig brain by three cycles of assembly according to Shelanski *et al.* (15) followed by phosphocellulose chromatography (16) in 25 mM MES, pH 6.6, 0.125 mM $MgCl_2$, 0.25 mM EGTA. Tubulin was concentrated by ultrafiltration in an Amicon cell and stored at −80 °C in 50 mM MES, pH 6.6, 0.5 mM EGTA, 0.25 mM $MgCl_2$, 0.1 mM GTP, 30% glycerol. Before each experiment, tubulin was polymerized to form microtubules in the presence of 6 mM $MgCl_2$, 0.5 mM GTP at 37 °C. The sedimented microtubules were resuspended at 0 °C in the polymerization buffer P used in the video-microscopy experiments (100 mM, PIPES, pH 6.8, 0.5 mM EGTA, 1 mM $MgCl_2$, 1 mM GTP). The tubulin solution was clarified by a 15-min centrifugation at 400,000 × *g* at 4 °C and kept on ice for the duration of the experiments (up to 6 h).

Axonemes were prepared from see urchin (*Sperikinus gralonairus*) sperm as described (17) and stored at −20 °C.

Light Microscopy—Samples were prepared for video-microscopy measurements as described (18). Axonemal pieces in P buffer were allowed to adhere for 20 s to the glass coverslip (22 × 22 mm). For experiments in which the curvature of microtubules in a flow of buffer was monitored, the coverslip formed the top of a flow cell of 180–220 μm thickness. A flux of buffer P was applied to the flow cell to remove the free axonemes, and tubulin was injected at the desired concentration in buffer P to allow microtubule assembly onto axonemal ends. Experiments were carried out at 37 ± 0.5 °C. Efficient thermostation of the cell and of solutions flowing through it was provided by a thermostat (Nikon) blowing warm air into a 30 × 30 × 40-cm Plexiglas chamber built around the objective + condenser + stage of the microscope.

Individual microtubules were observed in dark-field optical microscopy using a Reichert Polyvar microscope equipped with a plan apochromat-100 oil immersion objective lens (1.3 numerical aperture) and a 1.2–1.4 numerical aperture condenser. A 6-watt argon laser was used as a high intensity light source. The beam was guided through a multimodal optic fiber that was submitted to vibrational motion to eliminate speckle and obtain a homogeneous light distribution.

Images were detected using a silicon-intensified camera (Lhesa, LHL 046) connected to a Hamamatsu Argus 10 image processor and recorded in super SVHS format. The images of microtubules bending in a flow were digitized using Matrox hardware and a program kindly provided by Dr. Damien Schoëwaert. Roughly 25 points/microtubule were collected, over an average length of 20 μm. The points had coordinates (x, y) in the plane of the microtubule; the point of attachment of the microtubule to the axoneme was taken as the origin of axes, the flow was parallel to the y axis, and selected microtubules were initially (before the flow was applied) perpendicular to the direction of the flow. Therefore, the equation $y = 0$ described the shape of the straight microtubule in the absence of flow.

Measurements of Flexural Rigidity—Microtubules were considered as flexible hollow cylinders of length L, of inner and outer radii r_i and r_o, respectively. When attached by one end to the axoneme on the glass surface, microtubules can be constrained to bend within a plane by a flow of buffer applied in the flow cell. The flexural rigidity can be derived from the analysis of the shape of the microtubule at equilibrium in the solution, at a given flow rate. The experiment was performed as follows. In the absence of flow, microtubules having an orientation perpendicular to the direction y of flow were selected and their straight linear shape was recorded. A flow of buffer containing 10 μM tubulin (which is the critical concentration in P buffer) was then applied, which promoted bending of the microtubule to a new equilibrium position. At equilibrium, the internal stresses in the microtubule balance the external hydrodynamic forces. According to the linear elasticity theory (19), the energy of flexion of a circularly symmetric tubule is described by the following equation (linear elasticity theory of Landau and Lifshitz).

$$\varepsilon = \frac{K}{2}\int_0^L \left(\frac{d^2y}{dx^2}\right) dx \qquad \text{(Eq. 1)}$$

K is the flexural rigidity, and x and y are the coordinates of a current point along the microtubule length. Functional differentiation of Equation 1 leads to the force per unit length, f, acting at each point of the tubule.

$$f = K\frac{d^4y}{dx^4} \qquad \text{(Eq. 2)}$$

Microtubules grow from axonemes stuck on the glass surface of the coverslip. Since the geometry of the glass surface is not known at the microscopic level, we do not know whether microtubules can be considered as remaining in a plane parallel to the glass surface, or as growing out at a fixed angle to the surface, determined by the geometry of the microtubule. Near a solid surface, the velocity field of the flowing fluid increases linearly with the distance from the surface. Therefore, in the first hypothetical case (microtubule in a plane parallel to the surface), the microtubule feels a uniform force f along its length, while in the second case (microtubule at an angle to the surface) the microtubule feels a force that varies linearly with the position x along its length with a gradient f'. Two different differential equations describe these two cases: $f = K(d^4y/dx^4)$ for the first case, and $f'x = K(d^4y/dx^4)$ for the second case.

These differential equations must be solved with the following boundary conditions, expressing the absence of force or torque at the end of the microtubule.

$$\frac{d^2y}{dx^2} = 0 \quad x = L \qquad \text{(Eq. 3)}$$

$$\frac{d^3y}{dx^3} = 0 \quad x = L \qquad \text{(Eq. 4)}$$

The shape y (x) of the bent microtubule is described by the following equations (Equations 5 and 6), corresponding to the first and second cases, respectively.

$$y = \frac{fL^4}{24K}[(x/L)^4 - 4(x/L)^3 + 6(x/L)^2] \qquad \text{(Eq. 5)}$$

$$y = \frac{f'L^5}{120K}[(x/L)^5 - 10(x/L)^3 + 20(x/L)^2] \qquad \text{(Eq. 6)}$$

Bending was observed under conditions of hydrodynamic flow, such that the value of x at the end of the microtubule could be considered equal to L within 10%, which justifies the application of boundary conditions (Equations 3 and 4).

Whether the real situation corresponds to the theoretical first or second case can be determined by analyzing the microtubule length dependence of the deflection. The dependence is on the 4th power of the length in the first case (Equation 5), and on the 5th power of the length in the second case (Equation 6). According to the theory of polymer dynamics (20), the parameters f and f' are related to the properties of the flow and the fluid viscosity, ($\eta = 0.77 \times 10^{-3}$ kg m^{-1} s^{-1} for water at 35 °C), using the Oseen tensor to estimate the hydrodynamic flow around the microtubule. The following equations are obtained, corresponding to the two cases defined above, where d is the diameter of the microtubule.

$$f = \frac{4\pi\eta V}{\ln(L/2d)} \qquad \text{(Eq. 7)}$$

$$f = \frac{2\pi\eta V'}{\ln(L/2d)} \qquad \text{(Eq. 8)}$$

In the first case (Equation 7), V represents the velocity of the fluid evaluated in the plane of the microtubule. In the second case (Equation 8), V' represents the velocity gradient along microtubule length.

Equations 5 and 6 can therefore be rewritten as follows, showing the dependence of the shape on either fluid velocity (first case, Equation 9) or fluid velocity gradient (second case, Equation 10).

$$y = \frac{\pi\eta VL^4}{6K\ln(L/2d)}[(x/L)^4 - 4(x/L)^3 + 6(x/L)^2] \qquad \text{(Eq. 9)}$$

$$y = \frac{\pi\eta V'L^5}{60K\ln(L/2d)}[(x/L)^5 - 10(x/L)^3 + 20(x/L)^2] \qquad \text{(Eq. 10)}$$

The value of K can be derived by adjusting the theoretical curve to the digitized experimental curves. We have found that under a single set of experimental conditions, the shape of a bent microtubule could be described as well by Equation 9 or Equation 10. However, the length dependence expressed in the first term of the equations is different and allows to discriminate between the two models. The flexural rigidity, K, is the product of the Young's modulus, E, and of the geometrical moment of inertia of the cross-section of the microtubule. If we assume that the microtubule can be considered as a homogeneous cylinder of inner and outer radii r_i and r_o, respectively, the Young's modulus can be derived

from the measurements of flexural rigidity.

$$E = \frac{4K}{\pi(r_o^4 - r_i^4)} \qquad \text{(Eq. 11)}$$

Measurement of Microtubule Persistence Length—The flexural rigidity of microtubules can also be derived from measurements of the persistence length carried out in the absence of flow, *i.e.* under conditions of thermal bending. In these experiments, microtubules attached to axonemes were observed between the slide and the coverslip sealed together with valap, to avoid any fluid flow. The solution thickness between the two glass surfaces was 11 μm. When microtubules are attached to axonemes by one end and submitted to thermal forces in solution, the free end undergoes fluctuations around an average position. The average deviation, l, of the tip of the polymer, in a direction perpendicular to its average position, is related to the microtubule length, L, and to the persistence length, L_p (21), as follows.

$$l^2 = \frac{2}{3}\frac{L^3}{L_p} \qquad \text{(Eq. 12)}$$

The thermal fluctuations of microtubule free ends and the average position r_m were measured from the sequence of n video images of individual microtubules. The coordinates of the average position were defined by Equation 13.

$$r_m = \frac{1}{N}\sum_i r_i \qquad \text{(Eq. 13)}$$

To correct for possible net changes in length during measurements of r_i, the average projection of the fluctuation of the tip of the microtubule along a perpendicular r_m to the average position r_m was calculated as follows.

$$\langle l^2 \rangle = \frac{1}{N}\sum_i \left[\left(\overrightarrow{r_i - r_m} \right) \cdot \hat{r}_{m_\perp} \right]^2 \qquad \text{(Eq. 14)}$$

$(\overrightarrow{r_i - r_m})\cdot\hat{r}_{m\perp}$ is the scalar product of the vector representing the fluctuations, $(x_i - x_m, y_i - y_m)$, and of the normalized vector,

$$r_{m_\perp}\left(-y_m/\sqrt{x_m^2 + y_m^2}, x_m/\sqrt{x_m^2 + y_m^2}\right)$$

perpendicular to the microtubule average direction.

Microtubule Stabilization by BeF_3^-, H_2O, or AlF_4^-, and Taxol or Taxotere—Measurements of the dependence of the curvature of an individual microtubule on the force applied to it require its length to remain rigorously constant at all flow rates. This condition cannot be fulfilled easily due to the large fluctuations in length of standard microtubules at steady state (3). To circumvent this difficulty, microtubules can be stabilized by $[BeF_3^-, H_2O]$ or AlF_4^- structural analogs of inorganic phosphate (13), which have been shown to bind to the site of the γ-phosphate of GTP and to reconstitute a stable GDP-P_i-like microtubule, from which subunits dissociate at a very slow rate and which has lost its dynamic instability behavior.

Microtubules were allowed to grow off axonemes in the presence of 20 μM tubulin, until an average length of 10–20 μm was reached, then P buffer containing 10 μM tubulin (the steady state critical concentration) was flown through the cell, with a typical flow rate of 40 μl/min. Measurements of flexibility were then carried out on GDP microtubules at steady state. The flowing solution was then replaced by P buffer containing 5 μM tubulin, 150 μM of either $BeSO_4$ or $Al(NO_3)_3$, and 5 mM NaF. Measurements of flexibility were carried out after 15 min incubation in this buffer, for the binding of BeF_3^- or AlF_4^- to be completed (22).

For experiments in the presence of taxol or taxotere, microtubules were assembled off axonemes from 12 μM tubulin in P buffer containing 50 μM taxol or taxotere. Free microtubules formed by spontaneous nucleation were removed by a flux of P buffer containing taxol (100 μl/min for 10 min). The flexibility of taxol-bound microtubules attached to axonemes was then analyzed. Alternatively, microtubules were first assembled off axonemes in the absence of taxol, and then a flux of P buffer containing taxol was applied in the flow cell.

RESULTS

Evaluation of the Velocity of the Fluid in the Flow Cell and of Its Dependence on the Distance from the Glass Surface—The velocity of buffer flowing through the flow cell was evaluated by recording the movement of particles observed at a given focus in the flowing buffer. Fluid velocities were measured at different depths (z) within the solution. The z origin was arbitrarily chosen as the depth at which axonemes and attached microtubules were visible, *i.e.* the closest focus to the glass surface of the coverslip. The dependence of the fluid velocity on the distance, in the vicinity of the glass surface, is displayed in Fig. 1 for three different flow rates imposed by the pump. As expected, the fluid velocity increased linearly with the distance z from the glass surface in the range z = 0–5 μm. The plots of velocity *versus* distance (z) all converged to the same abscissa intercept at $z_0 = -0.35 \pm 0.1$ μm. This figure is consistent with the value of the diameter of sea urchin axonemes, which is 0.25 μm (23). At each depth, the observed particles are actually contained within a slice of fluid of thickness δz, which is the depth of focus. A slight gradient of fluid velocity exists within this slice. The distribution of the rates of particles gives an indication of the depth of focus of the microscope. This distribution is displayed in Fig. 1 (*inset*). The breadth of the distribution represents ±35% of the average velocity at 0.5 μm from the surface, which corresponds to a depth of focus of 0.35–0.40 μm. We note that the value of the depth of focus derived from the velocity measurements is in good agreement with the calculated value (24) corresponding to the high numerical aperture objective used here. From these observations, we can consider that microtubules attached to axonemes are constrained in a 0.4-μm-thick slice of solution, centered at a distance of ~0.3 μm from the glass surface. The maximum angle that a 20-μm-long microtubule can make with a plane parallel to the glass coverslip therefore is $\alpha = 0.4/20 = \pi/150 \sim 1°$. In all experiments described below, the value of the velocity represents the average value of ~10 measurements. In conclusion, at this point, the above observations favor the first model (see "Materials and Methods") according to which microtubules bending in the fluid flow are submitted to a constant hydrodynamic flow all along their length (as opposed to an increasing force upon going from the attached to the free end). However, other experiments, described in the following sections, have been designed to further discriminate between the two theoretical situations described under "Materials and Methods."

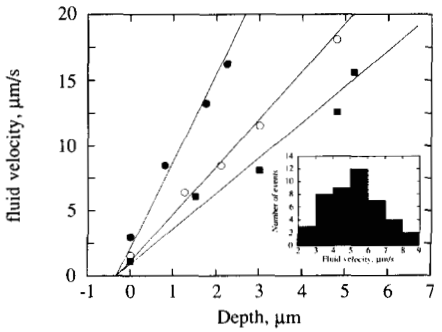

FIG. 1. **Dependence of the fluid velocity on the distance from the inner glass surface of the flow cell.** Buffer was flown through the flow cell using a peristaltic pump. Flow rates of 9.2 (*J*), 3.5 (*E*), and 1.8 (*B*) μl/min were imposed. Particles were observed by focusing at different distances from the glass surface of the coverslip. Fluid velocities were derived from the recorded trajectories. *Inset*, histogram of the distribution of fluid velocities measured at a depth of 0.5 μm from the glass surface (number of events = 45).

Analysis of the Bending of Individual Microtubules in a Hydrodynamic Flow: Effect of BeF_3^- on the Flexibility of Microtubules—In the absence of flow, microtubules attached by one end to axonemes appear as straight rods in dark-field microscopy (Fig. 2*A*). When a flow of buffer P containing 10 μM tubulin was applied perpendicularly to the microtubule axis, bending to an equilibrium position was observed (Fig. 2*B*). When the flow was stopped, the microtubules returned to their

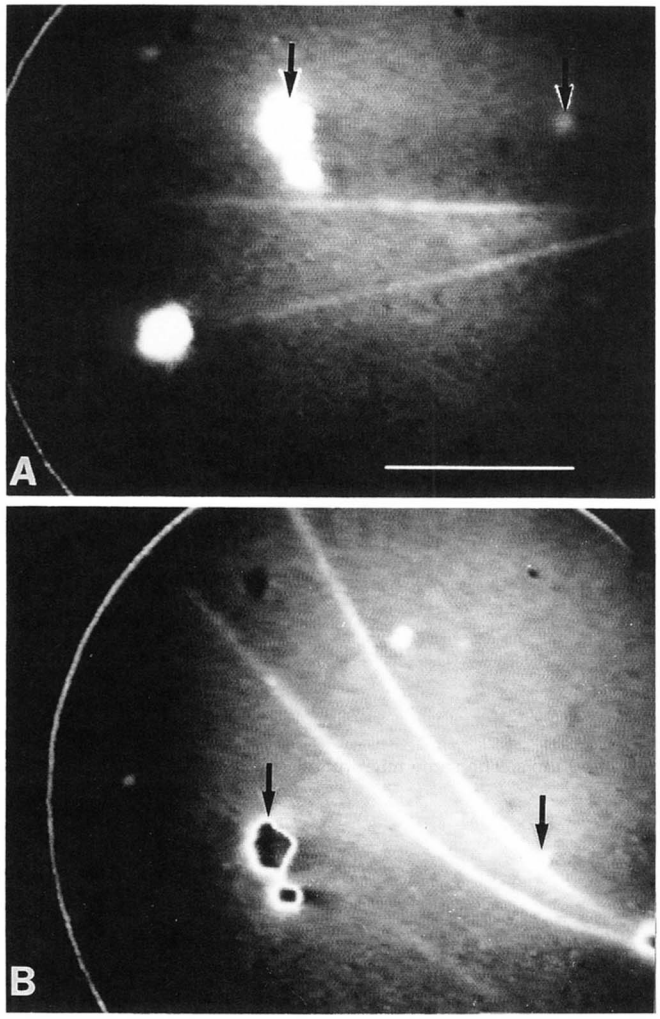

FIG. 2. **Dark-field images of microtubule bending in a flow of buffer.** *Panel A*, in the absence of flow, two microtubules attached to axonemes by one end display a straight shape. *Panel B*, the same microtubules bend in a flow of buffer. The flow rate was 40 μl/min, corresponding to a measured average fluid velocity of 50 μm/s in the vicinity of microtubules. *Arrows* point to bright immobile particles attached to the glass acting as landmarks in the field. *Bar*, 5 μm.

rest straight positions. When the flowing buffer contained 150 μM BeF_3, the shape of the same microtubule appeared straighter than in the absence of BeF_3^-. Fig. 3 shows that both in the absence and presence of BeF_3 at a given flow rate, the shape of the bent microtubule was well described by Equation 9. The value of the flexural rigidity could be derived from the fitted theoretical curve, knowing the values of L and of the flow rate measured in the same experiment at the depth of the microtubule. Series of measurements were carried out on microtubules of different lengths. For each microtubule, the flexural rigidity was measured both in the absence and in the presence of either BeF_3^- or AlF_4^-, which are structural analogs of P_i and equally stabilize microtubules in the GDP-P_i intermediate state of GTP hydrolysis (13, 22). The data, summarized in Table I, show that the value of the flexural rigidity was ~0.8–0.9 × 10^{-23} N × m^2 for GDP microtubules and 2.4–2.8 × 10^{-23} N × m^2 for either GDP-BeF_3 or GDP-AlF_4 microtubules. These figures correspond to values of the Young's modulus of ~0.5 and ~1.5 gigapascals for standard microtubules and GDP-BeF_3 microtubules respectively, assuming values of 14.2 and 11.5 nm for microtubule outer and inner radii, which are experimentally determined values (7) previously used by Gittes *et al.* (11) in flexibility measurements. These results indicate that the

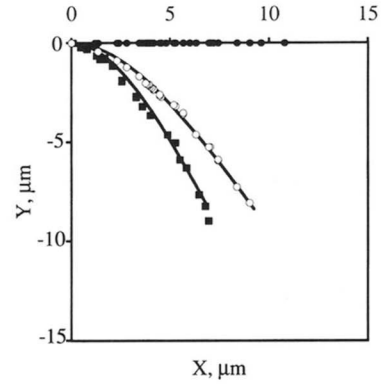

FIG. 3. **Analysis of the shape of GDP microtubules and GDP-BeF_3 microtubules bending in a hydrodynamic flow.** Symbols represent positions measured at different points (x, y) along the microtubule length. ●, microtubule at rest ($y = 0$) in the absence of flow; ■, GDP microtubule bending in the flow; ○, GDP-BeF_3 microtubule submitted to the same flow. The same microtubule is analyzed in the three situations. The origin ($x = 0$, $y = 0$) is the point of attachment of the microtubule to the axoneme. *Solid lines* are theoretical curves calculated according to Equation 9, with the following values of the parameters. $K = 0.82 \times 10^{-23}$ N × m^2 for standard GDP microtubule; $K = 2.2 \times 10^{-23}$ N × m^2 for GDP-BeF_3 microtubule. $r_o = 14.2 \times 10^{-9}$ m; $r_i = 11.48 \times 10^{-9}$ m; $L = 11 \times 10^{-6}$; $\eta = 0.77 \times 10^{-3}$ kg m^{-1} s^{-1} at 35 °C; $V = 42$ μm s^{-1}.

TABLE I
Flexural rigidity of microtubules derived from their bending in a hydrodynamic flow

Flexural rigidity was derived from the analysis of the bending shape of each microtubule of a given length, both under standard conditions (P buffer containing the steady-state critical concentration of 10 μM tubulin) and in P buffer containing 150 μM either BeF_3 or AlF_4. The average velocity of particles moving in the plane of the microtubule under study was measured in each single case.

Microtubule length	Fluid velocity	Flexural rigidity	
		+ BeF_3^-	Standard
μm	*μm/s*	*× 10^{-23} N × m^2*	
9.1	51	2.1	0.91
12.5	36	3.65	0.78
13	46	2.83	0.59
15.3	41	2.48	0.78
16.2	45	3.15	0.82
18.1	35	3.02	1.20
Average		2.9 ± 0.5	0.85 ± 0.2

Microtubule length	Fluid velocity	Flexural rigidity	
		+ AlF_4^-	Standard
μm	*μm/s*	*× 10^{-23} N × m^2*	
9.5	37	2.13	0.7
11.2	39	3.13	0.60
14.5	42	1.98	1.1
16.2	36	1.91	0.87
17.2	42	1.71	0.91
19	32	2.18	0.71
Average		2.5 ± 0.5	0.82 ± 0.18

decrease in polymer stability linked to P_i release (8, 22) is accompanied by a ~3-fold increase in microtubule flexibility.

Dependence of Microtubule Bending on Fluid Velocity—According to Equation 9, the deflection of the microtubule depends linearly on the fluid velocity. For a microtubule of a given length, Equation 9 can be written as follows:

$$y = A \cdot f\left(\frac{x}{L}\right)$$

where

$$A = \frac{\pi \eta V L^4}{6K \ln(L/2d)}$$

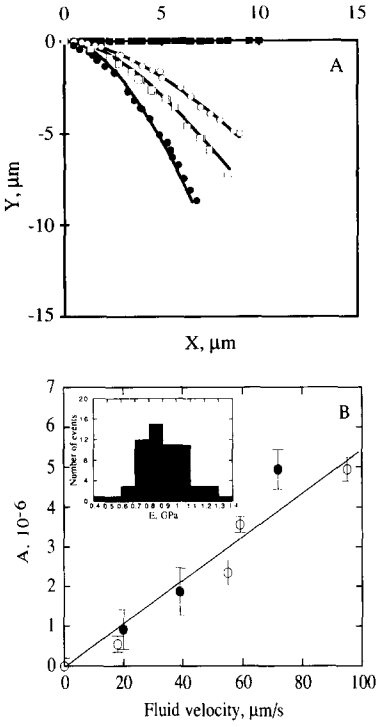

FIG. 4. **Dependence of microtubule deflection in the flow on fluid velocity.** *Panel A*, recorded equilibrium shapes of the same 10-μm-long GDP-BeF_3 microtubule submitted to three different flow rates. The following values of the fluid velocity in the plane of the microtubule were obtained (in μm/s): *B*, 0; *E*, 20; *G*, 39; *J*, 66. *Solid lines* are calculated according to Equation 9 with $K = 1.73 \times 10^{-23}$ N × m² for all curves. *Panel B*, dependence of the deflection on fluid velocity, for typical 10-μm-long microtubules. The value of the coefficient $A = \pi\eta VL^4/6K \ln(2d/L)$ (see text) was determined for two independent (● and ○) 10-μm-long GDP-BeF_3 microtubules, from the shape analysis at the indicated fluid velocities, as illustrated in *panel A*. The *straight line* fitting the data corresponds to a value of K of 1.73×10^{-23} N × m². The *error bars* indicate the standard deviation derived from 10 measurements of the microtubule fluctuating around its equilibrium position in the flow. *Inset*, histogram of distribution of the value of the Young's modulus, derived from cumulated measurements at different velocities and for the two microtubules (number of events = 61).

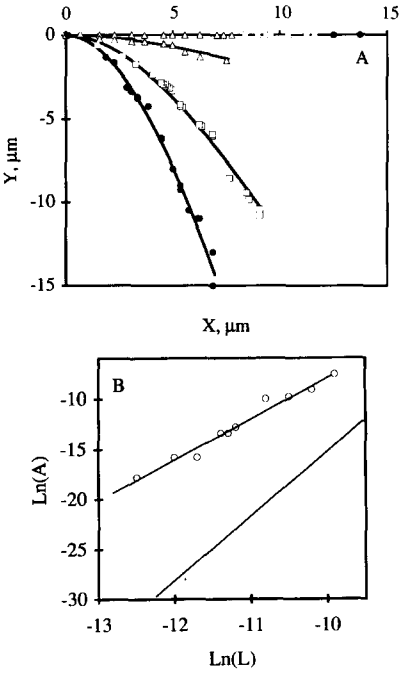

FIG. 5. **Length dependence of microtubule deflection in a hydrodynamic flow.** *Panel A*, recorded equilibrium shape of a single GDP-BeF_3 microtubule of different lengths and submitted to a constant flow of 40 μm/s. The same microtubule, initially 7.8 μm long (△), was allowed to grow up to 11.7 μm (□) and 13.8 μm (●) between deflection measurements, as described under "Materials and Methods." *Solid lines* are calculated fits according to Equation 9 using $K = 2.73 \times 10^{-23}$ N × m². *Panel B*, logarithmic representation of the length dependence of microtubule deflection. Each symbol represents the value of coefficient A derived from the shape analysis of microtubules of different lengths in the range 5.8–49 μm and bending in a flow of 40 μm/s. The *thick line* passing through the points has a slope of 4. The *thin line* drawn above has a slope of 5.

The linear dependence of A on V was tested by fitting Equation 9 to the shapes adopted by the same microtubule submitted to different hydrodynamic flows. These experiments were conducted in the presence of BeF_3^-, for microtubule length to remain rigorously constant during the time course of the experiment. Fig. 4*A* shows typical shapes recorded for a single microtubule in three different flows. The values of A were derived from the analysis of the shape taken at each flow rate. The data displayed in Fig. 4*B* for two 10-μm-long microtubules, show that A varied linearly with V in the range 0–90 μm/s. The fact that data corresponding to two different microtubules fall, within 20%, along the same straight line, testifies that the two microtubules were, within 20%, at the very distance from the glass surface at which the particles were observed to move in the flow. In other words, the error made on the value of K due to errors on the value of V cannot be larger than 20%.

At equilibrium in the fluid flow, the microtubule fluctuates around an average position. To estimate the uncertainty in the derived value of the Young's modulus, approximately 10 images of the microtubule at equilibrium were analyzed at each flow rate, leading to a histogram of distribution of the Young's modulus (Fig. 4*B*, *inset*), derived from measurements made at different velocities on different microtubules.

Length Dependence of Microtubule Bending in a Hydrodynamic Flow—As discussed under "Materials and Methods," the geometric disposition of the microtubule with respect to the glass surface is expected to affect the dependence of the deflection on the length of the microtubule. Very simply, if the microtubule is at an angle with the glass surface, the force of the fluid will display a steeper length dependence than if the microtubule is parallel to the glass surface. The length dependence of the microtubule deflection is in L^5 in the former case, in L^4 in the latter case. In the experiment shown in Fig. 5, a single microtubule was submitted to a constant flow (40 μm/s) and its shape was analyzed at different lengths. The increase in length was performed by increasing the concentration of tubulin in the buffer, at intervals sufficient for the microtubule to elongate to the desired length. The data were well described by equation 9 using the same value of K at all lengths. The logarithmic plot of A *versus* L (in the range 5–50 μm) had a slope of 4 (Fig. 5*B*). The dependence of the deflection on the 4th power of microtubule length establishes the validity of Equation 9 and the adequacy of the model according to which the microtubule is in a plane parallel to the glass surface.

Flexibility of Microtubules Stabilized by Taxol or Taxotere—Taxol is a drug (10) well known to bind preferentially to microtubules with high affinity. Taxotere is a biological precursor of taxol (14), which binds to and stabilizes microtubules as efficiently as taxol (25).[2] The bending of taxol- or taxotere-stabilized microtubules was assayed in a hydrodynamic flow as described above. Surprisingly, in the absence of flow, taxol-stabilized microtubules were not straight rods but exhibited a wavy, periodic shape. Typical dark-field images of taxol-stabilized microtubules are displayed in Fig. 6. Even in the absence

[2] P. Venier, A. C. Maggs, M.-F. Carlier, and D. Pantaloni, unpublished results.

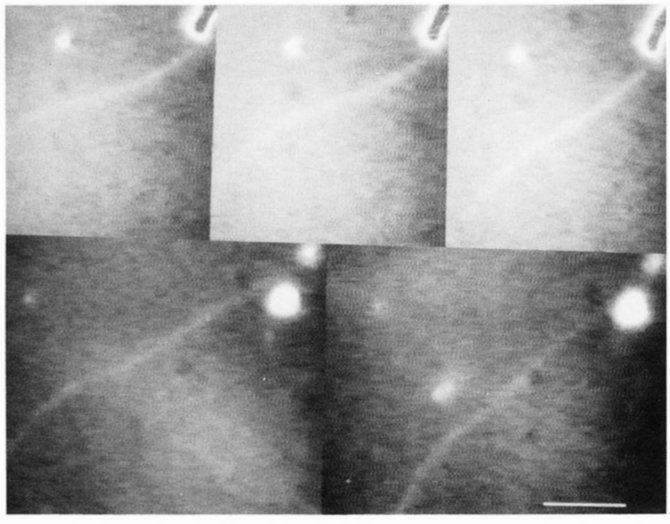

FIG. 6. **Dark-field images of taxol-stabilized microtubules.** Taxol-stabilized microtubules attached to axonemes were observed in the absence of flow. Note the wavy shape and frequent kink at 7 μm, presumably due to the three-dimensional helicoidal structure, observed in projection on a plane parallel to the coverslip. *Bar*, 2.5 μm.

of flow, the free end of these microtubules often went out of focus, indicating a higher flexibility than control microtubules. The digitized shapes of typical taxol and taxotere microtubules at rest, displayed in Fig. 7, show a half-period of about 7–8 μm. When a flow of buffer was applied, taxol microtubules bent to a very large extent and aligned parallel to the direction of the fluid even at fluid velocities as low as 5 μm/s. A similar very flexible appearance of taxol-stabilized microtubules in a flow of buffer has been reported (12). Bending of taxol-heated microtubules gliding over kinesin-coated surfaces has also been observed (26). All the above features, including periodic shape and frequent movement out of focus, suggest that taxol-treated microtubules may adopt a three-dimensional helicoid structure of ~15 μm pitch. The theoretical treatment developed under "Materials and Methods" to derive the Young's modulus from the bending in a flow only applies to semi-rigid linear rods undergoing deflections smaller than L, and hence was inadequate in the case of taxol-stabilized microtubules.

Evaluation of Microtubule Persistence Length from Measurements of the Thermal Fluctuations of the Free End of Axoneme-bound Microtubules—A static method therefore was elaborated to derive the value of the Young's modulus from measurements of the persistence length of taxol-stabilized microtubules attached to axonemes by one end. As described under "Materials and Methods," the persistence length of a semi-flexible rod attached at one end is correlated to the fluctuations of the free end around an average position. Taxol-stabilized microtubules may be considered as semi-flexible rods when their length is smaller than the half-period of the helicoid, *i.e.* in the range 0–7 μm. The persistence length L_p and the Young's modulus were calculated as described under "Materials and Methods." For each microtubule, 50–70 different positions of the tip at equilibrium were recorded, from which the value of l^2 was derived. Measurements were made on series of microtubules of different lengths, for standard GDP microtubules, for GDP-BeF_3 microtubules and for taxol-stabilized microtubules. Data, summarized in Table II, show that the persistence length of standard GDP microtubules is about 2 ± 0.2 mm, corresponding to a flexural rigidity of 0.92 ± 0.14 × 10^{-23} N × m^2, while for GDP-BeF_3 microtubules values of 6 ± 0.6 mm and 2.6 ± 0.16 × 10^{-23} N × m^2 were recorded. These two sets of data are in excellent agreement with the results of bending measurements in a hydrodynamic flow. Taxol- or taxotere-treated microtubules had

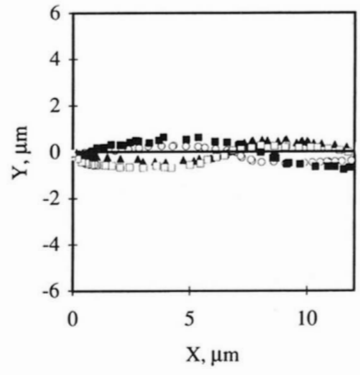

FIG. 7. **Recorded shapes of taxol- and taxotere-stabilized microtubules.** Typical ~15-μm-long microtubules were observed at rest. *Closed* and *open symbols* represent taxol- and taxotere-treated microtubules, respectively. Note the periodic appearance of these microtubules.

TABLE II

Persistence length and flexural rigidity of microtubules derived from thermal fluctuations of microtubule free end

Microtubules attached to axonemes at one end were observed at steady state under conditions of thermal equilibrium, in the absence (standard) or presence of either taxol or taxotere (10 μM) or BeF_3 (150 μM). For each microtubule, the mean equilibrium position and thermal fluctuations around it were derived from 50 ± 5 measurements of the position of the free end on recorded images, as described under "Materials and Methods."

Conditions	Microtubule length	Persistence length		Average flexural rigidity
		Measured	Average	
	μm	μm	μm	× 10^{23} N × m^2
Standard	15	1950	2200 ± 220	0.92 ± 0.09
	12	2329		
	8	2115		
	10	2400		
Taxol-stabilized	5	1170	1170 ± 100	0.47 ± 0.04
	3	1065		
	7	1243		
	8	1209		
Taxotere-stabilized	6	1179	1180 ± 130	0.48 ± 0.04
	5	1050		
	9	1228		
	4	1271		
Microtubule-GDP-BeF_3^-	11	6386	6100 ± 640	2.6 ± 0.27
	9	5870		
	15	6199		
	10	5945		

persistence lengths of 1.2 ± 0.12 mm corresponding to a flexural rigidity of 0.4 ± 0.1 × 10^{-23} N × m^2, *i.e.* were about 2-fold more flexible than standard microtubules. However these latter values should be taken with precaution, since they have been obtained within the assumption that 0–7-μm-long taxol-stabilized microtubules could be considered as rods bending in a plane, while observation of their three-dimensional helicoidal shape, in a range of longer lengths, is in contradiction with this model. All average values of flexural rigidity persistence length and Young's modulus obtained by the hydrodynamic and static methods for microtubules in different conformational states, are listed in Table III.

DISCUSSION

The present work is a novel experimental approach to the flexibility of microtubules and its possible role in microtubule function. Two independent methods have been used, a dynamic method in which the flexural rigidity is derived in a straightforward fashion from analysis of the bending of microtubules in

TABLE III

Comparison of the values of the physical parameters for microtubule flexibility derived from the dynamic and from the static methods

Methods M_1 and M_2 refer to the dynamic method (bending of microtubules in a flow of buffer) and to the static method (thermal fluctuations of microtubule free end), respectively.

	Standard		BeF_3^-/AlF_4^-		Taxol	
	M_1	M_2	M_1	M_2	M_1	M_2
Flexural rigidity ($\times 10^{23}$ N $\times$ m^2)	0.85 ± 0.20	0.92 ± 0.09	2.9 ± 0.5 2.5 ± 0.5	2.6 ± 0.27		0.49 ± 0.040
Persistence length (μm)	2000 ± 430	2200 ± 220	6850 ± 1300 5870 ± 1300	6100 ± 640		1170 ± 100
Young's modulus (gigapascals)	0.47 ± 0.10	0.51 ± 0.05	1.6 ± 0.30 1.37 ± 0.30	1.43 ± 0.15		0.27 ± 0.02

a hydrodynamic flow, and a static method in which the persistence length of microtubules attached at one end is derived from the thermal fluctuations of the free end. Both methods led to the same value (within 15%) of the flexural rigidity of standard microtubules, $K = 0.85 \pm 0.2 \times 10^{-23}$ N $\times$ m^2, which corresponds to a persistence length of 2000 ± 300 μm, which is in relatively good agreement with the range of values (700–1500 μm) given by Gittes *et al.* (11). The good agreement between the two methods used here validates the model and the analysis proposed for the deflection of microtubules in a flow. Indeed, the value of the flexural rigidity derived from the hydrodynamic method is highly dependent on the value of the fluid velocity. Although the fluid velocity is measured with accuracy at the same focus as the microtubule, within the depth limits of the fluid slice observed in focus, the fluid velocity varies by at least 60% (Fig. 1, *inset*). Therefore we should expect to observe variations of at least 60% in the flexural rigidity derived from measurements on different microtubules. Such large variations were not observed, and standard deviation was only 20%. This result means that microtubules can be considered as lying at a distance roughly constant (within ≤0.2 μm) from the glass surface, and submitted to a constant force corresponding to the average velocity measured. Similarly, we might have expected that microtubules attached to axonemes make a small angle with the glass surface. An angle as small as 1–2°, compatible with the depth of focus of the microscope, would result in a gradient of increasing velocity toward microtubule free end consistent with a 2-fold higher force at the tip than at the origin of the microtubule. The deflection that would be observed in this case however would not exhibit the L^4 dependence which is experimentally observed in a range of lengths from 5 to 50 μm. Therefore all data convey the view that microtubules are essentially lying in a plane parallel to the glass surface. Although the uncertainty on the value of V, however, remains the main source of uncertainty on the value of the flexural rigidity, this dynamic technique proves invaluable to measure small variations in flexibility linked to changes in buffer conditions, *i.e.* ligand binding, because the same microtubule can be observed under otherwise rigorously identical conditions (fluid velocity, geometry, position with respect to the glass surface, etc.). In principle, changes as small as 15–20% in flexural rigidity could be evaluated with accuracy.

Assuming that microtubules have outer and inner radii of 14.2 and 11.5 nm, respectively (*i.e.* a cross-sectional moment of inertia of 18.2×10^{-33} m^4), and that they are made of a homogeneous material, the Young's modulus of standard GDP microtubules is 0.5 ± 0.1 gigapascal. A variation of 1 nm (7%) in the value of r_o should be accompanied by a variation of 1.23 nm in the value of r_i ($r_o/r_i = \Delta r_i/\Delta r_o$, in order to keep the mass per microtubule unit length constant). It can be calculated that such a variation in r_o and r_i will result in a 20% variation in the value of the Young's modulus, which is the same order as the experimental error. Changes in microtubule protofilament number along a single microtubule have been reported (1). Such occurrences also cause ~20% change in the Young's modulus, which is not enough to be detectable as a discrete change in flexibility in an individual microtubule.

With both the dynamic and the static method, microtubules were found 3-fold more rigid in the presence of the phosphate analogs [BeF_3^-, H_2O] and [AlF_4^-], with values of $2.5–2.9 \times 10^{-23}$ N $\times$ m^2 for the flexural rigidity, corresponding to a persistence length of ~6 mm. This result indicates that in the intermediate GDP-P_i state of GTP hydrolysis in microtubule assembly, microtubules are more rigid than in the final GDP state. The previously documented (8, 13, 22) loss of polymer stability, which accompanies P_i release following GTP hydrolysis and is linked to a large change in tubulin conformation, now also appears to cause a large increase in microtubule flexibility. This is the first evidence that a reaction that is central to microtubule function (8) and responsible for oscillatory polymerization kinetics (27) is also associated to a large change in mechanical properties; hence, we may in turn wonder whether such changes in mechanical properties may be involved in the regulation of some biological functions of microtubules, *e.g.* the resistance to buckling forces exerted by motors involved in mitosis will be higher on GDP-P_i microtubules in a phase of rapid growth. It will be of interest to examine whether the flexibility of actin filaments is also affected by the bound nucleotide.

Taxol and taxotere, which are drugs known to stabilize microtubules, affect flexibility in a manner opposite to P_i analogs. In agreement with Dye *et al.* (12), we observed that microtubules bend more easily, *i.e.* seem to be more flexible than standard microtubules in a hydrodynamic flow. The same change was observed when microtubules were assembled onto axonemes in the presence of taxol and when taxol was added to pre-assembled microtubules. The change in flexibility appeared immediately following taxol addition, as was first observed by Dye *et al.* (12), indicating that the conformation change linked to taxol binding is fast. We also made the original observation that taxol binding induces a change in the three-dimensional structure of microtubules. Taxol-stabilized microtubules may no longer be considered as straight rods which can be constrained to bend in a plane, but seem to adopt the shape of a helicoid, of pitch ~15 μm and diameter ~1–2 μm. Such a shape can be generated by an accentuated skew of the protofilaments with respect to the microtubule axis, which could result from a conformation change of tubulin subunits affecting the lateral tubulin-tubulin contacts between protofilaments. In solution x-ray scattering, taxol-stabilized microtubules appear thinner, as made up of 12 protofilaments (28), which may be attributed to a decrease in the cross-section occurring in the skewing process. A clear interpretation of the present new findings obviously necessitates the detailed structural analysis of the microtubules lattice in the presence of taxol.

The discrepancy between the results of Dye *et al.* (12), who

concluded to an increased flexibility induced by taxol, and of Gittes *et al.* (11), who instead found an increased rigidity and persistence length of 5100 μm, is likely to be due to biases created by the different methodologies used. The change in the three-dimensional structure of the polymer from a rod to a helicoid certainly interferes with flexibility measurements using a hydrodynamic flow, since taxol-stabilized microtubules are no longer constrained in a plane, but their free end goes deeper into regions of the solution where the fluid velocity is higher; as a result, the greater apparent sensitivity of these microtubules to the flow gives the impression of a greater flexibility. Our measurements of flexibility using the static method indicate that the flexural rigidity (0.47×10^{-23} N × m^2) and persistence length (~1000 μm) of taxol- and taxotere-stabilized microtubules are only 2-fold lower than those of standard microtubules. In the thermal fluctuation measurements carried out by Gittes *et al.* (11), taxol-treated microtubules were forced to move in only two dimensions, since the thickness of the solution between the two glass surfaces was less than 3 μm. This constraint may have flattened the helicoidal superstructure, resulting in an apparent higher rigidity and a 5-fold larger value (5100 μm) of the persistence length. We note also that the amplitude of the fluctuations of a microtubule having a helicoidal superstructure depends on at least two elastic constants, the Young's modulus and the shear modulus (see Ref. 29 for a review).

In conclusion, the good quantitative agreement between the values of flexural rigidity of microtubules derived from two independent methods is encouraging for the future quantitative description of forces exerted by cytoskeletal elements in cell locomotion and shape changes. The present work also provides the first evidence for a connection between biochemical properties (biological function) of microtubules and their mechanochemical properties.

Acknowledgment—We thank Dr. Damien Schoëwaert for help in designing the image analysis software.

REFERENCES

1. Wade, R. H., Chrétien, D., and Jobs, D. (1990) *J. Mol. Biol.* **212,** 775–786
2. Mizushima-Sugano, J., Maeda, T., and Miki-Nomura, T. (1983) *Biochim. Biophys. Acta* **755,** 257–262
3. Horio, T., and Hotani, H. (1986) *Nature* **321,** 605–607
4. Cross, A. R., and Williams, R. C., Jr. (1991) *Cell Motil. Cytoskel.* **20,** 272–278
5. Amos, L. A., and Klug, A. (1974) *J. Cell Sci.* **14,** 523–549
6. Beese, L., Stubbs, G., and Cohen, C. (1987) *J. Mol. Biol.* **194,** 257–264
7. Chrétien, D., and Wade, R. H. (1991) *Biol. Cell* **71,** 161–174
8. Carlier, M.-F. (1989) *Int. Rev. Cytol.* **115,** 139–168
9. Murphy, D. B., Johnson, K. A., and Borisy, G. G. (1977) *J. Mol. Biol.* **117,** 33–52
10. Schiff, P. B., Fant, J., and Horwitz, S. B. (1979) *Nature* **22,** 665–667
11. Gittes, F., Mickey, B., Nettleton, J., and Howard, J. (1993) *J. Cell Biol.* **120,** 923–934
12. Dye, R. B., Fink, S. P., and Williams, R. C., Jr. (1993) *J. Biol. Chem.* **268,** 6847–6850
13. Carlier, M.-F., Didry, D., Melki, R., Chabre, M., and Pantaloni, D. (1988) *Biochemistry* **27,** 3555–3559
14. Bissery, M.-C., Guénard, D., Guéritte-Voegelein, F., and Lavelle, F. (1991) *Cancer Res.* **51,** 4845–4852
15. Shelanski, M. L., Gaskin, F., and Cantor, C. R. (1973) *Proc. Natl. Acad. Sci. U. S. A.* **70,** 765–768
16. Weingarten, M. D., Lockwood, A. H., Hwo, S. Y., and Kirschner, M. W. (1975) *Proc. Natl. Acad. Sci. U. S. A.* **72,** 1858–1862
17. Simon, J. R., Parsons, S. F., and Salmon, E. D. (1992) *Cell Motil. Cytoskel.* **21,** 1–14
18. Walker, R. A., O'Brien, E. T., Pryer, N. K., Soboeiro, M. F., Voter, W. A., Erickson, H. P., and Salmon, E. D. (1988) *J. Cell Biol.* **107,** 1437–1448
19. Landau, L. D., and Lifshitz, E. M. (1986) *Theory of Elasticity*, 3rd Ed., p. 187, Pergamon Press, Oxford
20. Doi, M., and Edwards, S. S. (1989) *The Theory of Polymer Dynamics*, p. 318, Oxford University Press, Oxford
21. Maggs, A. C., Huse, D. A., and Leibler, S. (1990) *Europhys. Lett.* **12,** 19–23
22. Carlier, M.-F., Didry, D., Simon, C., and Pantaloni, D. (1989) *Biochemistry* **28,** 1783–1791
23. Schrevel, J., and Besse, C. (1975) *J. Cell Biol.* **66,** 492–507
24. Inoué, S. (1986) *Video Microscopy*, p. 118, Plenum Press, New York
25. Diaz, J. F., and Andreu, J. M. (1993) *Biochemistry* **32,** 2747–2755
26. Amos, L. A., and Amos, W. B. (1991) *J. Cell Sci. Suppl.* **14,** 95–101
27. Carlier, M.-F., Melki, R., Pantaloni, D., Hill, T. L., and Chen, Y. (1987) *Proc. Natl. Acad. Sci. U. S. A.* **84,** 5257–5261
28. Andreu, J. M., Bordas, J., Diaz, J. F., Garcia del Ancos, J., Gil, R., Medrano, F. D., Nogales, E., Pantos, E., and Towns-Andrews, E. (1992) *J. Mol. Biol.* **226,** 169–184
29. Marko, J. F., and Siggia, E. D. (1994) *Macromolecules* **27,** 981–988